Materials Research Bulletin 179 (2024) 112909

Contents lists available at ScienceDirect

Materials Research Bulletin

journal homepage: www.elsevier.com/locate/matresbu

Research Papers

Synthesis of TiO_2 nanoparticles by green approach: Application as photoanode for dye-sensitized solar cells

Anamika Chaudhari, Aman Kumar, Sudhanshu Kumar, Suman Kushwaha *

Department of Chemistry, Institute of Science, Banaras Hindu University, Varanasi, Uttar Pradesh 221 005, India

ARTICLE INFO

Keywords:
TiO_2 NPs
Aloe barbadensis miller
Green approach
X-ray diffraction
Raman spectroscopy

ABSTRACT

Efficient photoanodes play a central role in the performance of dye-sensitized solar cells. Traditional methods for synthesizing TiO_2 often involve chemical processes that can be expensive and environmentally harmful due to the use of toxic and hazardous substances. Therefore in this work, TiO_2 nanoparticles (NPs) were synthesized using bio-inspired processing through a hydrothermal procedure using different concentrations of *Aloe barbadensis miller* leaves extract as the reducing and stabilizing agent. Scanning electron microscopy (SEM), UV–vis spectroscopy (UV), X-ray difraction (XRD), Raman Spectroscopy, transmission electron microscopy (TEM) and Brunauer–Emmett–Teller (BET) analysis were used to characterize as synthesized TiO_2 NPs. DSSCs were fabricated employing the prepared TiO_2 NPs as photoanodes, and their performance was assessed. DSSC generates J_{SC} of 9.7 mA/cm^2, V_{OC} of 0.682 V and efficiency (η) of 4.3 % when 20 mL concentration of extract was used for the synthesis of TiO_2 NPs and subsequently their photoanodes.

1. Introduction

Dye sensitized solar cells (DSSCs) have appeared as a promising alternative to traditional silicon-based photovoltaic solar cells in the global search for sustainable energy sources [1–6]. DSSCs have indeed garnered significant attention from researchers and the solar energy community due to several advantageous features that set them apart from traditional solar cell technologies such as; low-cost, flexible structure, ease of fabrication, lightweight etc. However, it's important to note that DSSCs also faces challenges, such as lower efficiency compared to some other solar cell technologies, potential issues with long-term stability, and sensitivity to environmental factors. Despite that, researchers challenge to focus on the lacking aspects (enhance efficiency, stability, and scalability for practical applications) of DSSC with solemn attention because of its promising nature. The initial work on DSSCs is often attributed to the efforts of Hishiki and Gerischer in the 1960s, where they employed zinc oxide (ZnO) as a semiconductor and sensitizing dyes (rose Bengal & cyanine) to capture light energy [7,8]. In 1977, the Spitler & Calvin [9] group replaced ZnO with titanium dioxide (TiO_2) as the semiconductor material. This switch to TiO_2 significantly improved the efficiency and stability of DSSCs. In 1991 by Michael Gratzel and Brian O′ Regan fabricated DSSC and achieved efficiency of 7.1 % [10]. First, O'regan and Grätzel fabricated DSSCs using Ru-based dyes as sensitizers and mesoporous TiO_2 NPs film as the photoanode. The other photo-anode of wide bandgap of metal oxides such as ZnO, ZrO_2, CuO and SnO_2 etc. are also commonly used. The photoanode is a critical component of DSSCs, and its material greatly influences the device's performance. Several materials have been used as the photoanode material for DSSC but TiO_2 remains one of the most capable materials for the photoanode in DSSCs due to its combination of favourable properties. Its widespread use is indeed driven by factors such as cost-effectiveness, abundance, non-toxicity, and its ability to provide a large surface area for dye adsorption. Further, because of its small particle size, high surface area, low density, high electron mobility and high band gap energy, TiO_2 play an important role [11–13]. The high surface area of TiO_2 NPs enhances the interface between the semiconductor and the dye, promoting efficient light absorption and electron injection. This is essential for the overall performance of the DSSCs. The high electron mobility and excellent conductivity of TiO_2 facilitate the rapid transport of electrons from the dye molecules to the conductive substrate, contributing to the overall efficiency of electron transfer in DSSCs. TiO_2 exists in different crystalline phases, with anatase being one of them. The anatase phase of TiO_2 is highly active for electron transfer, making it favourable for DSSC applications. TiO_2 NPs have been synthesized using various methods, each with its own set of advantages and limitations. The choice of synthesis method often

* Corresponding author.
E-mail address: sumankush@bhu.ac.in (S. Kushwaha).

https://doi.org/10.1016/j.materresbull.2024.112909
Received 1 February 2024; Received in revised form 1 May 2024; Accepted 18 May 2024
Available online 20 May 2024

depends on the desired properties of the TiO_2 NPs and the intended applications. Some methods are sol-gel, hydrothermal, emulsion precipitation, solvothermal, flame combustion [14–19] etc. The majority of these methods are highly costly and required toxic chemicals. Therefore, recent research has highlighted the effectiveness of plant extracts in the synthesis of TiO_2 NPs. Green synthesis methods utilizing plant extracts offer several advantages, including lower cost, sustainability, and reduced environmental impact. Several plant extracts have been used to synthesis TiO_2 NPs, including Jatropha curcas Annona squamosa, Psidium guajava, Desmodium gangeticum, Solanum trilobatum, Mangifera indica, Carica papaya, Jatropha curcas L, Eclipta prostrata, Camellia sinensis [20–30]. In this work, TiO_2 nanostructures were synthesized by the green synthesis method utilizing *Aloe barbadensis miller* leaves extract as reducing agents and showed its application in DSSC as photoanode. The plant extracts can act as a reducing and a stabilizing agent in the synthesis of TiO_2 NP in addition to impart its intrinsic properties contributed by the polysaccharides, flavanones, terpenoids [31–33] etc. Synthesis of TiO_2 NPs using *Aloe barbadensis miller* leaves extract have been performed by some researchers [34–44] but to the best of our knowledge no one shows its application in DSSCs after preparing NPs. Table 1 listed the application of *Aloe barbadensis miller* mediated TiO_2 NPs for its various applications.

In our work, TiO_2 NPs have been synthesised using different concentration of *Aloe barbadensis miller* leaves extract as reducing agent. The as synthesised NPs were coated over FTO substrates and they were utilized as photoanode after sintering. DSSCs were fabricated, and its photovoltaic performance was investigated. In this work, for the sensitization of TiO_2 commercial N719 dye was used as sensitizers.

2. Materials and procedures

2.1. Materials

Fresh and fully-fledged leaves of *Aloe barbadensis miller* plant were plucked from the kitchen garden. Titanium isopropoxide (99.9 %) and Triton-X (Triton™ X-100, laboratory grade) were bought from Sigma Aldrich, India. Solvents Isopropyl alcohol (anhydrous, 99.5 %, ethanol (absolute, ≥99.5 % (GC)), acetlyacetone (Reagent Plus®, ≥ 99 %) polyethylene glycol, (PEG (average M_n 400)) and sodium hydroxide (NaOH) were bought from Merk India. Fluorine-doped tin oxide conductive glass (FTO, transmission ≥ 83 %, sheet resistance 15 Ω/sq), Pt solution, electrolyte (EL-HPE high performance electrolyte) solution, N719 dye, sealant (60 μm, Meltonix 1170-60) were bought from Bat-Sol equipment technology, India.

2.2. Different constituents of Aloe barbadensis miller

Aloe vera (*Aloe barbadensis miller*), a member of the Asphodelaceae family (formerly Liliaceae), is a perennial plant with turgid green leaves joined at the stem. The gel extracted from the leaves of *Aloe barbadensis miller* is about 98.5 %–99.5 % water and rich in a variety of compounds such as phenolic anthraquinones, flavonoids, flavonols, and enzymes. *Aloe barbadensis miller* contains various polyphenolic compounds, which are plant-derived compounds with antioxidant properties [45,46]. Different chemical constituents present in plan are shown in Fig. 1.

2.3. Preparation of Aloe barbadensis miller leave extract mediated TiO_2 NPs

A 150 g of washed and dried *Aloe barbadensis miller* leaves were peeled, finely cut and boiled in 500 mL of water (double distilled). The subsequent extract ready to use for the preparation of TiO_2 NPs [47]. Four separate TiO_2 precursor solution were prepared in four different flask by drop wise addition of 3 mL of TTIP (Titanium isopropoxide) in 100 mL distilled water under continuous magnetic stirring and 20 mL, 40 mL, 60 mL and 100 mL of above *Aloe barbadensis miller* leave extract was added separately in each precursor solution simultaneously. The mixture was retained under constant stirring on a magnetic stirrer for 4 h continuously at 100 °C and then cooled and filtered. Obtained materials were washed with water over and over again to remove the by-products and residual parts and subjected to centrifugation process and particles were washed again with distilled water and preserved in oven at 80°C for 12 h. The dried powder was crushed into fine powder in mortar using mortar and subjected to anneal at 450 °C for 1.5 h in a tubular furnace. 20 mL, 40 mL, 60 mL and 100 mL concentration of *Aloe barbadensis miller* leave extract based synthesized TiO_2 NPs were coded as TiO_2-av20, TiO_2-av40, TiO_2-av60, TiO_2-av100 respectively in further studies.

2.4. Assembly of DSSCs

For fabricating photo anode the paste of each prepared NPs; TiO_2-av20, TiO_2-av40, TiO_2-av60, TiO_2-av100 were prepared individually by mixing 0.5 g of prepared TiO_2 powder in and 0.2 mL Triton-X in a mortar and finely grinded. Further, 0.03 mL acetyl acetone and 0.3 mL of PEG (polyethylene glycol) was added to the mixture and grinded gradually to make smooth paste. The prepared four TiO_2 pastes was spread homogeneously over the four different cleaned FTO substrate using doctor blade technique and dried at moderate temperature and annealed for 1 h at 450°C to obtain the photoanodes for sensitization. Photoanode using pure TiO_2 powder (Aldrich) was also prepared following the same procedure and used for comparison. Same thickness of all thin films were maintained using scotch tape. The prepared TiO_2 thin films were immersed overnight in the N719 dye solution separately for complete dye adsorption and used as photo-anode in the DSSCs. The amount of adsorbed dye has been measured from the UV-Vis absorbance spectra of the dye desorbed into 1 N NaOH solution (ethanol–H_2O (1:1, v/v)). Beer–Lambert law (A = ε.c.l) was used to calculate the dye molecules

Table 1
Summarizes the application of *Aloe barbadensis miller* mediated TiO_2 NPs for its various uses.

S. No	NPs	Precursor	Method	Shape of NPs	Application of synthesized NPs	Refs.
1.	TiO_2	Titanium Chloride ($TiCl_4$)	Hydrothermal	Spherical Size ~ 20 nm	Valuation of its antibiofilm potential against *Pseudomonas aeruginosa* PAO1	[37]
2.	TiO_2	Titanium Chloride ($TiCl_4$)	Hydrothermal	Irregular structure Size ~ 20 nm	No application	[35]
3.	TiO_2	Titanium Chloride ($TiCl_4$)	Hydrothermal	Spherical.	Nano-drug delivery system for the anticancer drug, doxorubicin (Dox).	[39]
4.	TiO_2	Titanium (IV) tetrabutoxide	Sol -gel	Spherical with Agglomeration. Size ~ 100 nm	No application	[40]
5	TiO_2	Titanium Chloride ($TiCl_4$)	Hydrothermal	Spherical Size ~ 13-22 nm.	No application	[41]
6	TiO_2	Titanium isopropoxide	Hydrothermal	Spherical Size ~ 15-50 nm.	Radio sensitization	[38]
7	TiO_2	titanium tetraisopropoxide	Hydrothermal	Spherical Size ~ 5-6.9 nm.	Therapeutic	[42]
8	TiO_2	Titanium Chloride ($TiCl_4$)	Hydrothermal	Spherical, Size ~ 25 nm.	TiO_2 – PANI nanocomposite	[43]
9	TiO_2	Titanium isopropoxide	Sol-gel	Nanocoral	No application	[44]

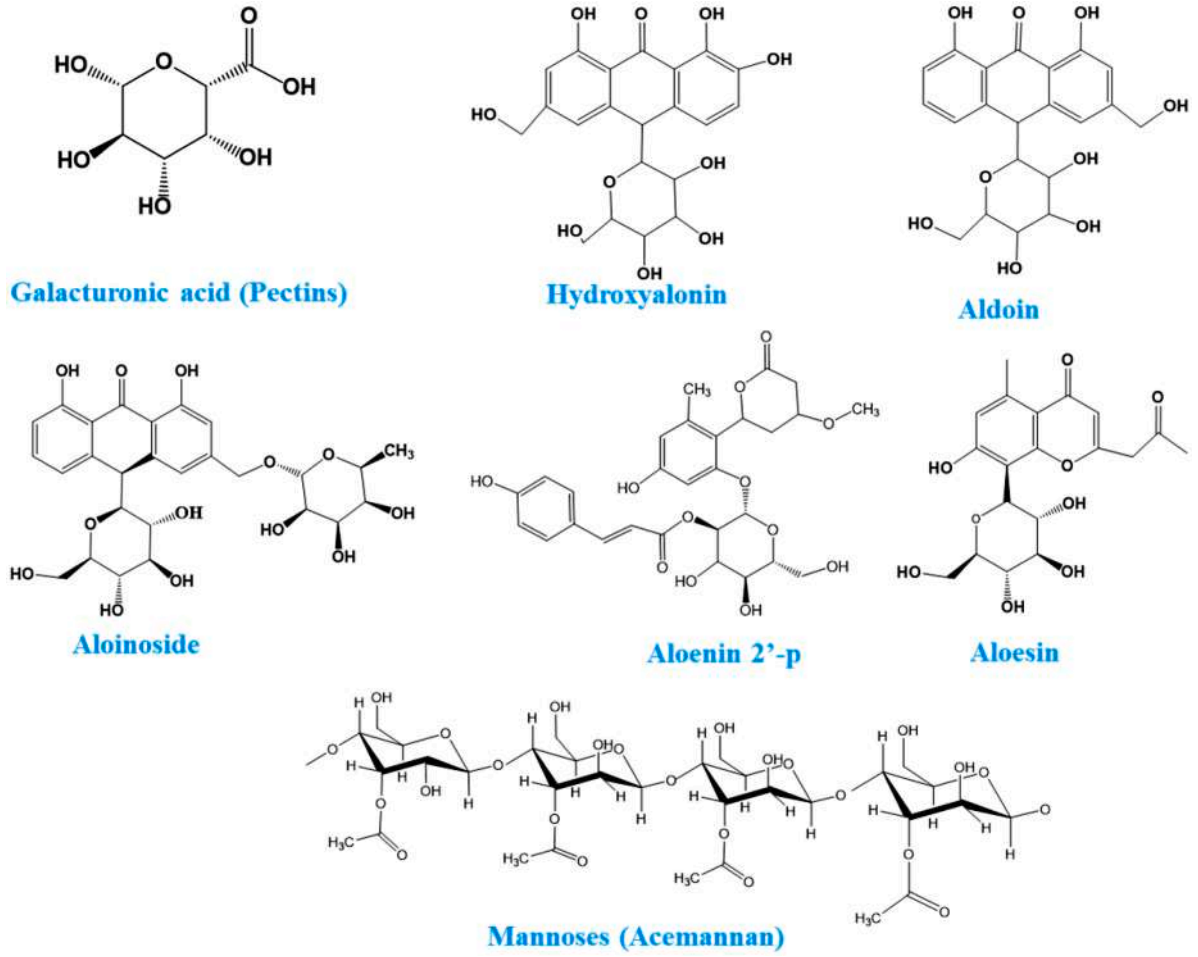

Fig. 1. Important chemical constituents of *Aloe barbadensis miller*.

adsorbed into the photoanode. Where, A is the absorbance, ε is the molar extinction coefficient of dye, c is the concentration of solution, and l is the length of optical pat. The Pt counter electrodes were prepared by doctor blade method by spreading commercial Pt paste on cleaned FTO glass and finally annealed for 1 h at 400°C. Two electrodes were joined together through a sandwich type configuration for DSSC. Finally, the gap between the electrodes was filled with the electrolyte. The fabricated DSSCs were coded as DSSC/TiO_2-av20, DSSC/TiO_2-av40, DSSC/TiO_2-av60, and DSSC/TiO_2-av100 for different concentration of *Aloe barbadensis miller* leave extract (20 mL, 40 mL, 60 mL and 100 mL) mediated TiO_2 NPs based DSSCs respectively. DSSCs based on pure TiO_2 powder was coded as DSSC/TiO_2. The *J-V* and EIS investigations of the prepared devices were carried out under 1 sun illumination.

2.5. Instruments

To analyse the crystalline state, X-ray diffraction (XRD) studies of synthesized TiO_2 NPs were carried out at 2∨ in the range of 20-80 °C using X-ray diffractometer (D8 Advance (Eco) Bruker. Raman spectroscopy studies were carried out using a laser confocal Raman microscope (LabRAM HR Evolution by Horiba Inc.).The UV-Vis absorption spectra was done using a UV/Vis spectrophotometer (UV-1900i, Shimadzu Corporation, Japan). The surface morphology was analyzed using scanning electron microscope (JSM – 7500, JEOL, Tokyo, Japan). TiO_2 NPs morphology were examined using a transmission electron microscope (TECNAI 20Gˆ2 FEI, Thermofisher company). Brunauer-Emmett-Teller (BET) analysis was performed using (Quantachrome Instruments (USA), Autosorb (IQ2)). Electrochemical measurements (EIS) were recorded using Metrohm Autolab (Multi Autolab M204) module controlled by NOVA 2.10 software from 100 kHz to 0.1 Hz with 10 mV amplitude under open-circuit conditions. A class Solar Simulator of 1000 W Xenon arc lamp with AM 1.5 G filters (SL-50A-WS, Sciencetech, Canada) was used as light source at 1 sun light intensity of 100 mW/cm^2 to carried out Current-potential (*J-V*) studies. An active cell area at 0.25 cm^2 was fixed for illumination by masking.

3. Results and discussion

3.1. Crystallographic analysis

Debye-Scherer's equation and the Williamson-Hall (W-H) plot are both important tools in the characterization of crystalline materials using X-ray diffraction techniques [48–50]. While both methods involve the measurement of diffraction peaks, they offer complementary approaches to understanding different aspects of the crystalline material. Debye-Scherrer's equation primarily focuses on estimating crystallite size, while the Williamson-Hall plot allows for the analysis of multiple factors contributing to peak broadening, including crystallite size and lattice strain. In Williamson-Hall plot, the width of diffraction peaks is plotted against the scattering angle, often represented as the sine of the angle (sin θ), where θ is the angle of incidence of the X-ray or neutron beam. The broadening of peaks in diffraction patterns can arise from various factors, including crystallite size, strain, and lattice defects. The Williamson-Hall plot helps to separate these contributions by providing a linear relationship between the peak broadening and the reciprocal of the crystallite size or lattice strain. The linear equation for the

Williamson-Hall plot is: $\beta \cdot \cos(\theta) = K \cdot \lambda$. Where, β is the full width at half maximum (FWHM) of the diffraction peak, θ is the Bragg angle, K is a constant that depends on the crystallite shape and strain distribution, and λ is the wavelength of the incident radiation. By analyzing the slope and intercept of the linear plot, one can extract information about the average crystallite size and the strain present in the material. A steeper slope might indicate a larger contribution from strain broadening, while a larger intercept might suggest smaller crystallite sizes. Debye--Scherrer's equation is derived from the Bragg's law for diffraction, which states that for constructive interference to occur, the path difference between two adjacent crystallographic planes must be an integer multiple of the wavelength of the incident X-rays. When applied to a powder sample with randomly oriented crystallites, the Debye-Scherrer equation provides a means to estimate the average crystallite size from the broadening of the diffraction peaks in the X-ray diffraction pattern. The equation is given by: $D = \frac{K\lambda}{\beta \cos\theta}$. where, D is the average size of the crystalline particles in the direction perpendicular to the scattering plane (often referred to as the crystallite size or grain size), λ (λ = 1.5406 Å for Cu-source) is the wavelength of the incident X-rays, K is a dimensionless shape factor constant, typically around 0.9 for spherical particles and varies for other shapes, β is the full width at half maximum (FWHM) of the diffraction peak, θ is the Bragg angle. The plane spacing d is related to the lattice constants a, c and the Miller indices by the equation $\frac{1}{d^2_{(hkj)}} = \frac{4}{3}\left(\frac{h^2+hk+k^2}{a^2}\right) + \frac{l^2}{c^2}$. . Where, d_{hkl} is the plane spacing, and h, k, l are Miller indices.The XRD patterns of NPs (TiO_2-av20, TiO_2-av40 TiO_2-av 60 and TiO_2-av100) synthesized using different concentrations of *Aloe barbadensis miller* leave extract (20 mL, 40 mL, 60 mL and 100 mL as reducing agents are shown in Fig. 2. The XRD peak intensity in *Aloe barbadensis miller* leave extract mediated TiO_2 are slightly sharper, compare to pure TiO_2 powder which indicates the formation of a highly crystalline NPs and this could be due to the effective stabilization of NPs by the phytomolecules of *Aloe barbadensis miller*. The XRD pattern of all the TiO_2 NPs exhibit tetragonal crystal structure with diffraction peaks indexed matches with the anatase phase of TiO_2 NPs (JCPDS card No.: 21-1272). The other peaks observed in the XRD patterns can be indexed to (004), (200), (105), and (204), (220), (215), (312) planes of the samples. The particle size of the green synthesized TiO_2 NPs for the (101) peak is calculated using Debye- scherrer's equation and ranged from 8-12 nm. TiO_2 NPs size decrease with the increase in concentration of reducing agent which may be probably due to the increase of reduction process with the increase of *Aloe barbadensis miller* leave extract concentration [51].

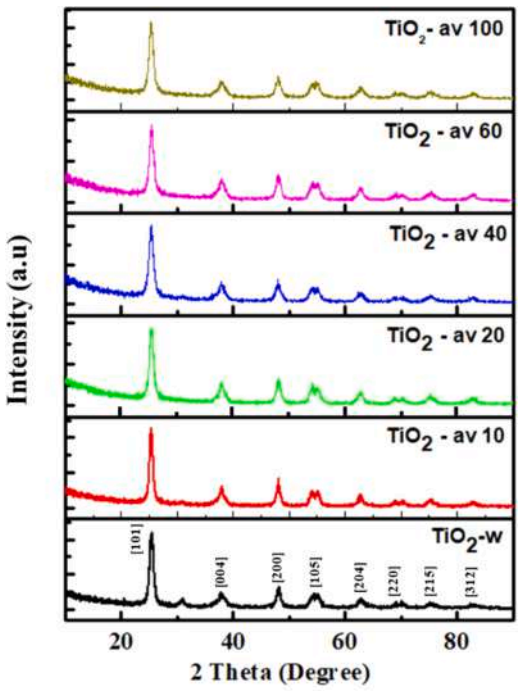

Fig. 2. XRD pattern of TiO_2 NPs (TiO_2-av20, TiO_2-av40 TiO_2-av60 and TiO_2-av100) prepared with 20 mL, 40 mL, 60 mL and 100 mL concentrations of *Aloe barbadensis miller* leaves extract respectively. XRD pattern of pure TiO_2 NPs (black line).

3.2. Raman analysis

The structural phase transformation, crystalline behaviour and purity of synthesized TiO_2 NPs were further analysed by Raman spectroscopy technique, based on the vibrational modes detected in the spectrum. The Raman spectra of the synthetized TiO_2 NPs with different concentrations of *Aloe barbadensis miller* leave extract are given in Fig. 3. Raman spectra of pure TiO_2 NPs is also shown (black line). As seen from Fig. 3, there are four major vibration modes were observed in the spectrum, and these vibration modes were associated with the confirmation of the crystalline anatase phase transformation of TiO_2 NPs. The peak immersed at 640.3 cm^{-1} (Eg) due to the Ti-O stretching mode. The peak situated at 518 cm^{-1} ($A_{1g} + B_{1g}$) could be due to Ti-O stretching mode while the peak at 397 cm^{-1} (Eg) could be due O-Ti-O bending mode [52]. The crystalline nature and peak intensity were greater for green synthesized TiO_2 NPs (mainly TiO_2-av 20 sample) compared to TiO_2 pure NPs (TiO_2). This could be due to the change of the crystal size in *Aloe barbadensis miller* leave extract synthetized TiO_2 NPs with different concentrations [53].

3.3. Optical properties

To investigate the effect of *Aloe barbadensis miller* extract concentration on the absorption spectra of TiO_2 NPs, UV-Vis spectroscopy was used for spectral analysis and the same is shown in Fig. 4. All green synthesized TiO_2 NPs samples have absorption spectra in the range of 300-400 nm. Pure TiO_2 NPs typically exhibit a characteristic absorption peak in the range of 320−350 nm [54]. The concentration of the any

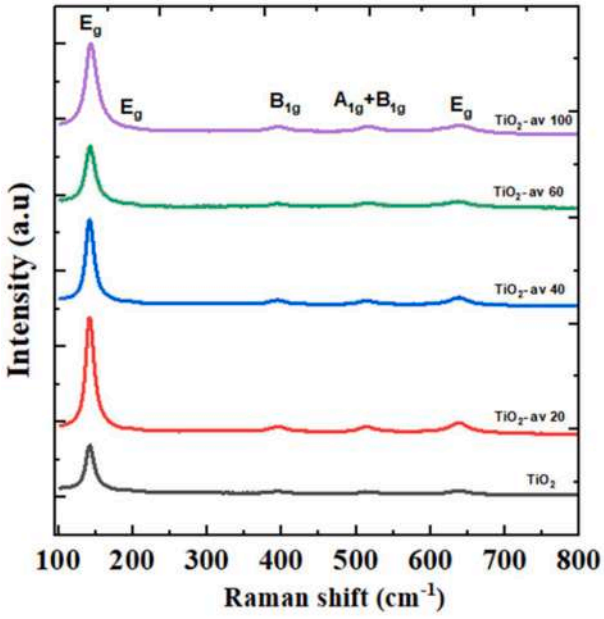

Fig. 3. Raman spectra of synthesized NPs (TiO_2-av20, TiO_2-av40 TiO_2-av60 and TiO_2-av100) prepared with 20 mL, 40 mL, 60 mL and 100 mL concentrations of *Aloe barbadensis miller* leaves extract respectively. Raman spectra of pure TiO_2 NPs is also shown (black line).

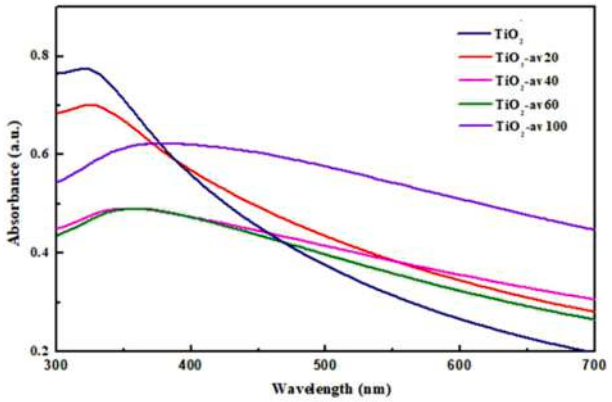

Fig. 4. UV−vis spectra of synthesized NPs (TiO_2-av20, TiO_2-av40 TiO_2-av60 and TiO_2-av100) prepared with 20 mL, 40 mL, 60 mL and 100 mL concentrations of *Aloe barbadensis miller* leaves extract respectively. UV−vis spectra of pure TiO_2 NPs is also shown.

green extract used in the synthesis of NPs can significantly influence the characteristics and properties of the resulting NPs, such as; size, morphology, crystallinity, surface area, and photoelectrochemical properties including their absorption and scattering characteristics. Although, higher concentrations of the green extract typically lead to faster reduction rates due to increased availability of reducing agents. Higher concentrations may promote greater nanoparticle aggregation, leading to broadening or red-shifting of absorption peaks due to plasmonic coupling effects. However, there is typically an optimal concentration range beyond which further increases may not necessarily improve the efficiency and could even lead to adverse effects such as aggregation of molecules or increased charge recombination. Finding this optimal concentration often involves experimental optimization and may vary depending on the specific green extract and TiO_2 NPs characteristics. Optimal concentrations may lead to enhanced photoelectrochemical properties by providing a balance between efficient reduction and proper surface functionalization. Here, in our studies using *Aloe barbadensis miller* extract for the synthesis of TiO_2 NPs, the optimized concentration was when 20 mL concentration of *Aloe barbadensis miller* leaves extract was used (TiO_2-av20). Although maximum absorbance was seen when 100 mL concentration of *Aloe barbadensis miller* leaves extract (TiO_2-av100) was used this is often attributed to the increased presence of reducing agents or stabilizing agents from the green extract but due to aggregation of molecules and increased charge recombination, less *J*sc and overall efficiency was achieved compared to 20 mL concentrations. Since the photocurrent density depends on the amount of dye loaded on the TiO_2 films, quantification was carried out by dye desorption followed by UV-visible analysis, as described in the experimental section. The amount of dye adsorbed on the TiO_2-av20 photoanode (44 nmoles/cm^2) was higher than bare TiO_2 photoanode (36 nmoles/cm^2) and generate a higher photocurrent density (Table 3). Optimal concentrations may lead to enhanced photoelectrochemical properties by providing a balance between efficient reduction and proper surface functionalization. Further increase in the concentration of *Aloe barbadensis miller* leaves extract the dye loading amount decreases which is probably because of aggregation of molecules and increased charge recombination and therefore less *J*sc and overall efficiency (η) was achieved compared to 20 mL concentrations.

3.4. SEM and TEM analysis

Surface and the particle morphology of with and without *Aloe*

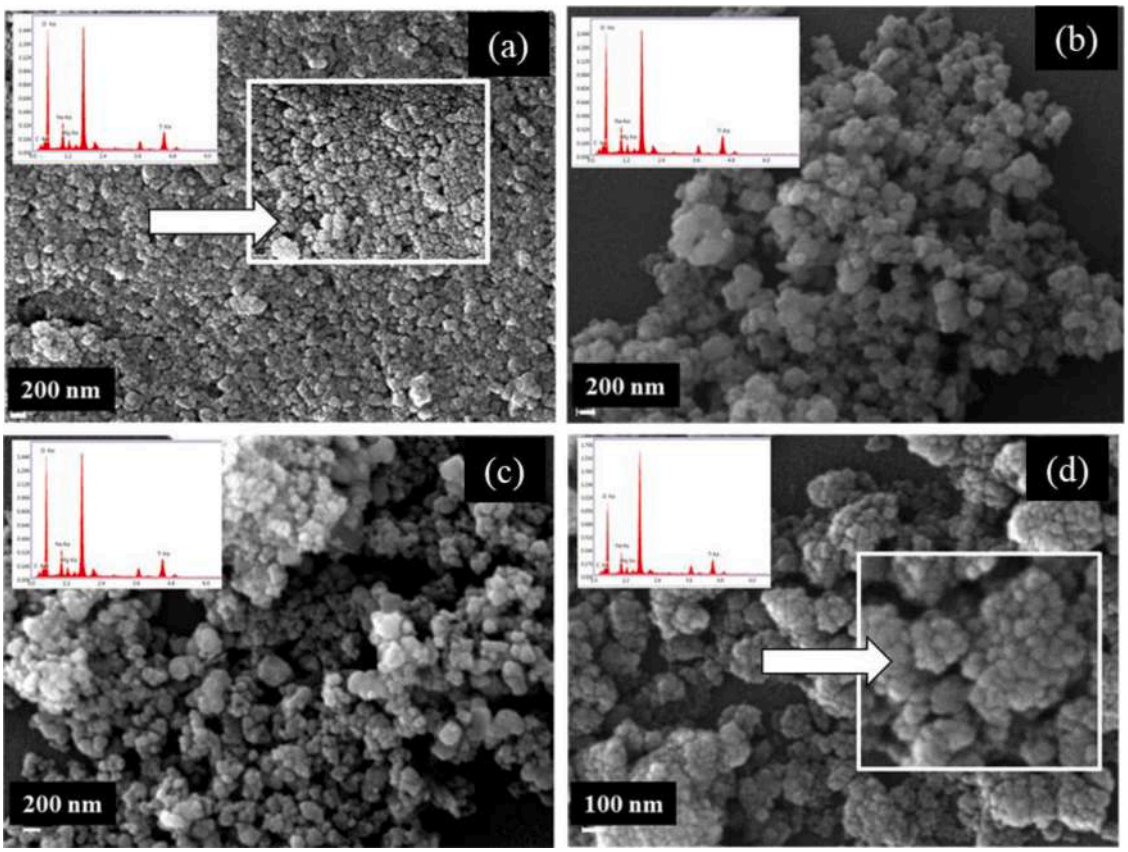

Fig. 5. FE-SEM images of TiO_2 NPs prepared with different concentrations of Aloe barbadensis miller leaves extract; (a)- TiO_2-av20, (b)-TiO_2-av40 and (c)-TiO_2-av60, (d)-TiO_2-av100. Corresponding the EDAX is also shown in inset.

barbadensis miller leaves extract mediated TiO_2 NPs were investigated by SEM analysis (Fig. 5). It can be seen from the Fig. 5 (a–d) that *Aloe barbadensis miller* leaves extract has a significant impact on the control of agglomeration and reduction in the particle size of TiO_2 NPs. thus, *Aloe barbadensis miller* leaves extract appears to have a positive impact on the control of agglomeration, reduction in particle size, and the formation of shaped controlled synthesis of TiO_2 NPs. SEM images represent that there is a well-associated interaction between biomolecules and TiO_2 NPs during the synthesis process and indicates that during the synthesis process, spherical-shaped TiO_2 NPs were formed, The elemental analysis of the chemical compounds was investigated through EDS spectra (energy dispersive X-ray spectroscopy) and shown in Fig. 5 (inset). The presence of Ti and O peaks could be considered as a successful indication of the synthesis of TiO_2 NPs and as expected in there are strong peaks of C, O, K and Mg etc. besides Ti and O, indicate that the extracellular organic moieties are adsorbed on the surface of the metallic nanoparticles. Elements Mg, C, O and K mainly come from the composition of *Aloe barbadensis miller* leaves extracts. TiO_2 NPs having the size ranged between 10-15 nm. The HRTEM images are shown in Fig. 6 and reveals that the TiO_2 NPs are interconnected are composed of nanocrystallites with a width of ~13 nm. SAED patterns of the synthesized TiO_2 NPs show a polycrystalline nature (Fig. 6).

3.5. BET analysis

The BET (Brunauer-Emmett-Teller) method is extensively used method for determining the specific surface area of materials based on N_2 adsorption-desorption isotherms [55]. Fig. 7. Shows the characteristic plot of N_2 adsorption-desorption isotherm and pore size distribution curves for *Aloe barbadensis miller* leaves extract mediated TiO_2 NPs. The corresponding pore-size distribution (BHJ) of the as-prepared TiO_2 NPs is presented in Fig. 7 (b). The as synthesized TiO_2 NPs displayed the isotherm of type-IV with hysteresis loops at relative higher pressure range of 0.55–1.0 which shows the absorption bevavior of the green synthesized NPs. The pore size distributions indicated that TiO_2 presented a relatively wider distribution ranging from 40 to 60 nm.

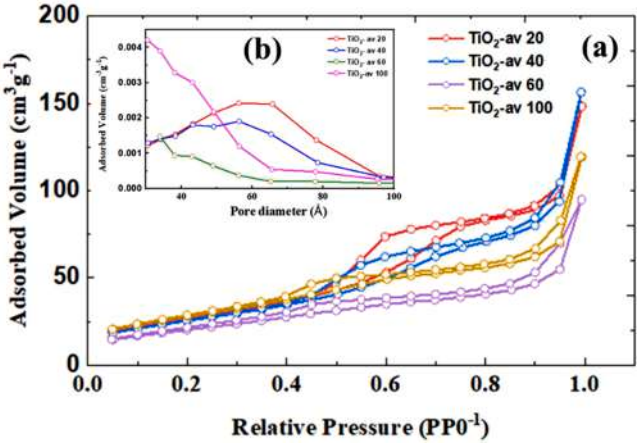

Fig. 7. N_2 adsorption isotherms and pore size curves (inset) of the TiO_2 NPs prepared with different concentrations of *Aloe barbadensis miller* leaves extract.

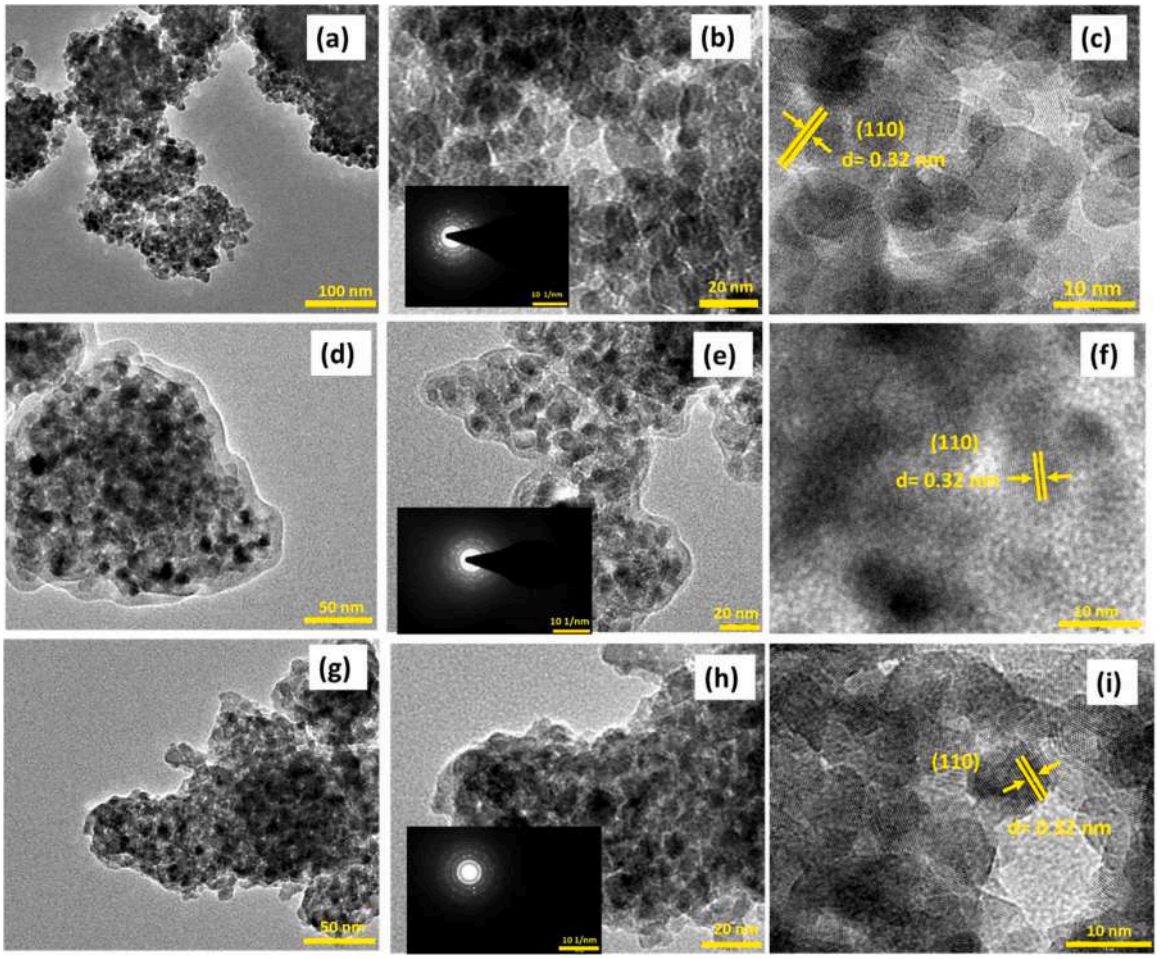

Fig. 6. FE-TEM images of synthesized TiO_2 NPs prepared with various concentrations of *Aloe barbadensis miller* leaves extract; TiO_2-av20 (a-c), TiO2-av40 (d-f) and TiO_2-av60 (g-i). Corresponding the SAED pattern is also shown in inset.

With increase in concentration of *Aloe barbadensis miller* leaves extract the peak at 60 Å is reduced, indicating that the average pore size decreases as the concentration of reducing agent increases from 20 ml to 100 ml (Fig. 7 inset). All prepared samples show very high surface areas (Table 2), which are substantially larger than that reported for commercially available P25 (50 $m^2 g^{-1}$) [56]. The high BET surface area could ease the dye-loading capacity and might give the DSSCs higher short-circuit current density (*Jsc*). The specific surface areas of TiO_2 NPs synthesized with different concentration of TiO_2 are 76.361 m^2g^{-1}, 71.658 m^2g^{-1}, 31.583 m^2g^{-1} and 53.699 m^2g^{-1}. The decrease in the surface area with increase in concentration of reducing agent was expected as the increase the surface area is probably due to presence of increase in capping agents on the NPs. The mesoporous nature, large surface area of the green-synthesized TiO_2 NPs make them promising candidate for dye adsorption for DSSCs application.

3.6. Measurement of photovoltaic performance and EIS spectra

(a) J–V photovoltaic analysis

To explore the photovoltaic properties of the *Aloe barbadensis miller* leaves extract mediated TiO_2 NPs, we fabricated DSSCs and *J-V* plot is shown in Fig. 8[A]. For comparison DSSC was also fabricated using pure TiO_2 based photoanode. The assembled different DSSCs were evaluated under the illumination of 100 mW/cm^2 light intensity. Actual illuminated portion of the cell was 0.25 cm^2. The fill factor (FF) and efficiency (η) of the fabricated DSSCs were estimated using the equations given by; $FF = \frac{J_{max}\ X\ V_{max}}{J_{sc}\ X\ V_{oc}}$, $\eta\ (\%) = \frac{V_{oc} \times J_{sc} \times FF}{I_{inc}}\ x\ 100$. Where J_{max} and V_{max} were obtained at the maximum power output in the *J-V* plot. J_{SC} is short-circuit current density (mA cm^{-2}), and V_{OC} stands for the open-circuit voltage, respectively. I_{inc} is the power of incident light. The current–voltage (*J–V*) characteristics are largely dependent on the series (*Rs*) and shunt (*Rsh*) resistance [57]. *Rs* arises from various factors including contact resistance at interfaces, bulk resistance, charge transfer resistance in semiconductor material, and sheet resistance of electrodes. Higher *Rs* diminishes the fill factor, thereby reducing the maximum power output of the solar cell. Optimizing *Rs* is crucial for enhancing solar cell performance. *Rsh* provides an alternative current path for photo-generated current and is linked to electron recombination at the semiconductor/dye/electrolyte interface, often due to crystal defects in semiconductor material. Low *Rsh* leads to significant power loss in the solar cell. Maintaining a sufficiently high *Rsh* is essential for minimizing power loss [57]. The values of series and shunt resistances was determined from the *J–V* curve (Fig. 8[A]). The values of *Rs* and *Rsh* can be determined from the *J-V* curve, typically depicted in Fig. 8(A), using specific relations. *Rs* is calculated as the slope of the *J-V* curve at zero voltage, $R_s = \left(\frac{\Delta V}{\Delta J}\right)_{V=0}$, while *Rsh* is calculated as the slope of the *J-V* curve at zero current $R_{sh} = \left(\frac{\Delta V}{\Delta J}\right)_{j=0}$. The photovoltaic parameters; open circuit voltage (V_{OC}), short circuit current density (J_{SC}), fill factor (*FF*) and conversion efficiency (η) are given in Table 3. The maximum *Jsc* = 9.7 mA/cm^2 and overall conversion efficiency (η) = 4.2 % was obtained for DSSC/TiO_2- av20 followed by DSSC/TiO_2–av40, which is higher than DSSC/TiO_2. The higher photocurrent for DSSC/TiO_2-av20 device might be because of well-dispersed nanoparticles with interconnected networks, which facilitate efficient electron transport and reduce resistive losses, contributing to higher DSSC efficiency. Secondly, higher specific surface area providing sufficient dye-loading to the surface of TiO_2 for more light harvesting [58]. Thus, optimal concentrations can promote efficient charge separation at the dye/TiO_2 interface, minimizing charge recombination and maximizing electron injection into the TiO_2 conduction band, which are crucial for achieving high DSSC efficiency. The larger value of *Rs* in the case of DSSC/TiO_2 and DSSC/TiO_2-av20 device is responsible for its relatively more deviation from the ideal *J–V* characteristics. But, the higher value of *R*sh in the case of /TiO_2-av20 based DSSC may be responsible for its high performance then DSSC/TiO_2.

Table 2
Surface area analysis of synthesized TiO_2 NPs.

Sample	BET Surface area (m^2g^{-1})	Pore Volume (cm^3g^{-1})	Pore Size (nm)
TiO_2-av20	76.361	0.229	2.8174
TiO_2-av40	71.658	0.226	2.4514
TiO_2-av60	31.583	0.126	1.6999
TiO_2-av100	53.699	0.156	1.5254

The obtained photoelectrochemical results were similar to those reported in previous works [59–66]. In our recent work we have obtained J_{SC} = 9.72 mA/cm^2, V_{OC} = 660 mV and FF = 0.46 and efficiency of 3.0 %, with the DSSC fabricated with green tea mediated TiO_2 NPs based photo anode [59]. Shalini et al. [60] report synthesis of TiO_2 NPs using Citrus limon juice extract which act as a green-capping agent to control the shape, size and agglomeration behaviour of the growing TiO_2 NPs and obtained an efficiency of 4.55 % compared to uncapped TiO_2 (1.31 %). Raj Kumar et al. [61] prepared TiO_2 nanostructures via green route using the fruit extracts derived from pineapple, orange, and grapes as reducing agents respectively and used as photoanode in DSSCs and obtained an efficiency of 3.89 % with orange extact. Maurya et al. [62] synthesized mesoporous anatase TiO_2 NPs using Bixa orellana seed extract and further used it for making DSSC photoanode and achieved an efficiency of 2.97 %. Sharif et al. [63] used facile green modified solvothermal method to prepare pristine TiO_2 and Ag-doped TiO_2 with 1, 2, 3, and 4 % of Ag and obtained an efficiency of 2.45 % when 4 % Ag-TiO_2 was used as phoroanode. Table 4 shows performances of DSSCs using different natural extract mediated TiO_2 photoanodes by other research groups.

(b) Transient photocurrent - time profile

Analysing the transient photocurrent-time profile is a valuable approach to understanding the response of prepared photoanodes to a photon trigger and assessing the sustainability of the short-circuit current in a DSSC. When a photon triggers the absorption of light by the dye molecules in the photoanode, it initiates the generation of charge carriers (electrons and holes). The transient photocurrent-time profile reveals how quickly and effectively the photoanode responds to this photon trigger. A rapid increase in photocurrent following the photon trigger indicates efficient light absorption, charge separation, and collection processes within the photoanode. The sustainability of Isc over time, as observed in the transient photocurrent-time profile, reflects the ability of the photoanode to continuously generate and transport charge carriers in response to incident light [67]. Thus to understand the response of prepared photoanodes to a photon trigger and assessing the sustainability of the short-circuit current the study was performed on all the fabricated DSSCs and same is shown in Fig. 8[B]. It can be seen that in all the fabricated DSSCs, a sudden and sharp rise in short-circuit photocurrent was seen when light was put 'ON' to illuminate the device. The maximum photocurrent conquered initially was slightly decayed during the illumination time of ~ 50 s. While, in the light 'OFF' condition the photo current abruptly dropped down (as in dark current). Thus from transient photocurrent - time profile it can be concluded that the rate of dye regeneration is fast enough to keep up with the injection of charge carriers by excited dye molecules. This implies efficient utilization of the dye molecules and effective regeneration of the dye in the presence of the redox couple.

(c) Electrochemical Impedance analysis

Electrochemical Impedance Spectroscopy (EIS) is influential

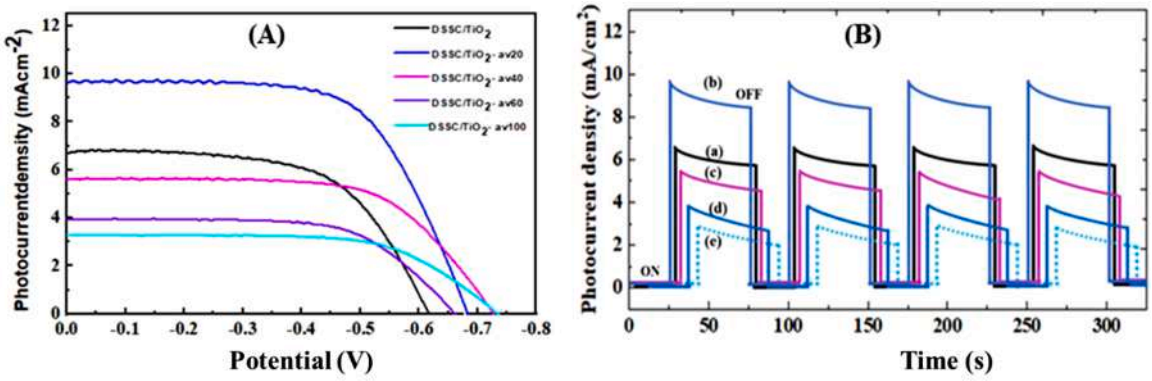

Fig. 8. [A] *J-V* plot, [B] transient current-time (*J-t*) graph of different DSSCs based on TiO_2 photoanode prepared with various concentrations of *Aloe barbadensis miller* leaves extract under. (Light intensity = 100 mW cm^{-2}).

Table 3
Summarizes the dye loading amount, photovoltaic parameters, (R_s) and (R_{sh}) values of DSSCs with different photoelectrodes.

Devices	Dye loading (nmoles/cm^2)	J_{SC} (mA/cm^2)	V_{OC} (V)	FF	η (%)	R_S/Ω cm^2	R_{Sh}/Ω cm^2
DSSC/TiO_2	36±3	6.7±0.003	0.616±0.002	0.62±0.018	2.5±0.15	50	863
DSSC/TiO_2-av20	44±3	9.7±0.002	0.682±0.003	0.60±0.016	4.3±0.13	47	1573
DSSC/TiO_2-av40	27±1	5.6±0.002	0.727±0.001	0.64±0.014	2.6±0.11	23	2120
DSSC/TiO_2-av60	24±2	4.0± 0.001	0.661±0.002	0.64±0.015	1.7±0.12	22	1944
DSSC/TiO_2-av100	22±1	3.3±0.001	0.735±0.002	0.63±0.013	1.5±0.14	16	2372

Table 4
Performances of DSSCs using different natural extract mediate TiO_2 NPs and subsequently their photoandes.

Plant/ natural /extract	Synthesis technique	Photoanode	Counter Eletrode	Jsc (mAcm^{-2})	Voc (V)	FF	η	Refs.
Citrus Limon	Sol - gel	TiO_2	Pt	3.42	0.61	0.63	1.31	[60]
		C-TNP		7.00	0.691	0.82	3.87	
		C'-TNP		9.10	0.776	0.65	4.55	
		C''-TNP		5.89	0.722	0.64	2.73	
Orange	Sol - gel	TiO_2 + N719	Pt	8.80	0.569	0.57	3.35	[61]
		O- TiO2 + N719		9.00	0.649	0.66	3.89	
Bixa orellana	Sol - gel	TNP	Pt	2.0	0.680	0.73	1.03	[62]
		G-TNP		9.0	0.506	0.65	2.97	
Fig Leaf	Sol- gel	4% Ag- TiO_2	Pt	8.33	0.698	0.422	2.45	[63]
Phellinus linteus mushroom	Sol-gel	TiO_2	Pt	8.18	0.69	0.67	3.80	[64]
Halomonas sp. RAM2		NDSSC $_{BIO(5)}$	Pt	2.72	1.06	0.39	0.048	[65]
		NDSSC $_{BIO(10)}$		1.24	2.13	0.47	0.44	
		NDSSC $_{BIO(15)}$		8.92	5.95	0.27	0.0088	
		NDSSC $_{P25(10)}$		1.78	1.84	0.28	0.55	
Saccharum officinarum	Sol – gel	Uncapped TiO_2 (C1)	Pt	2.03	0.46	0.73	0.69	[66]
		Capped TiO_2 (C2)		2.94	0.61	0.72	1.29	
		Capped TiO_2 (C3)		7.65	0.68	0.68	3.65	
Aloe barbadensis miller	Hydrothermal	DSSC/TiO_2	Pt	6.7	0.616	0.62	2.5	Our work
		DSSC/TiO_2-av20		9.7	0.682	0.60	4.3	
		DSSC/TiO_2-av40		5.6	0.727	0.64	2.6	
		DSSC/TiO_2-av60		4.0	0.661	0.64	1.7	
		DSSC/TiO_2-av100		3.3	0.735	0.63	1.5	

technique used to study the dynamics of electron transport and recombination in various electrochemical systems, including semiconductor materials like TiO_2 NPs used in DSSCs. EIS provides information about the electrical properties of a system by measuring its impedance response to an applied AC voltage over a range of frequencies. Fig. 9 shows the electrochemical impedance spectra (Nyquist plot) of different DSSCs under open circuit voltage (V_{OC}) illuminated with solar light intensity of 100 mW cm^2 and a frequency range from 1 Hz to 10 kHz. An equivalent circuit is shown in the inset of Fig. 9 to represent EIS, which consists of electrical components of sheet resistance Rs, charge transfer resistance R_{CT1} and R_{CT2}, and electrochemical capacitance CPE1 and CPE2 for first and second semicircle of the Nyquist plot respectively. Rs resistance is related to the sheet resistance on the FTO substrates and the contact resistance between TCO and TiO_2. Usually, three semicircles are produced in the EIS of DSSCs. The semicircle in high frequency region signifies the charge transfer resistance (R_{CT}) at the electrolyte/counter-electrode interface (R_{CT2}), the second semicircle is due to electron transfer at the TiO_2/dye/ electrolyte (R_{CT1}), interface and the third semicircle seen in the low frequency region correspond to diffusion of the redox electrolyte [68,69]. Fig. 9 shows the Nyquist plot of the DSSCs fabricated with different photoanodes, which shows the

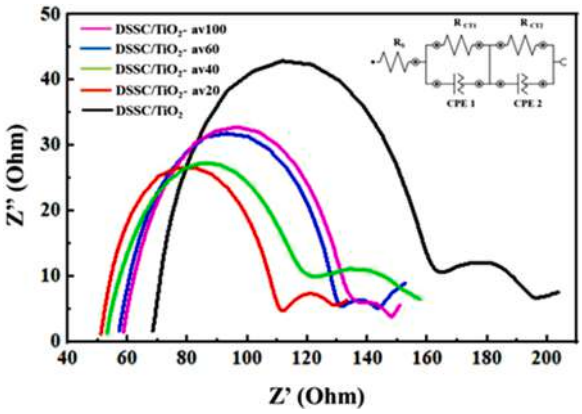

Fig. 9. Nyquist plots of DSSCs based on TiO_2 photoanode prepared with different concentrations of *Aloe barbadensis miller* leaves extract under open circuit voltage condition. The equivalent circuit used is shown as an inset.

overlapping of first and second semicircles of high and middle frequencies and it could be associated with the low resistance of the counter electrode (Pt) [70]. The series resistance (*Rs*) value was obtained to be 68.40 Ω, 54.00 Ω, 57.60 51.10 Ω, 52.90 Ω for DSSC/TiO_2, DSSC/TiO_2-av20, DSSC/TiO_2-av40, DSSC/TiO_2-av60 and DSSC/TiO_2-av100 respectively. The series resistance (*Rs*) was observed to be increased for the DSSC/TiO_2. Though, a small difference in *Rs* values was noticed for the DSSC/TiO_2-av20, DSSC/TiO_2-av40, DSSC/TiO_2-av60 and DSSC/TiO_2-av100 which corresponds to the contact resistance. This reduction in Rs is probably due to photoelectrode surface enhancement due *Aloe barbadensis miller* leaves extract. The charge transfer resistance at the counter electrode / electrolyte interface (R_{CT1}) was varied, which could be associated with the different counter electrodes used to assemble the DSSCs [71]. The R_{CT1} value was obtained to be 48.70 Ω, 19.70 Ω, 22.5, 28.5 Ω, 47.60 Ω for DSSC/TiO_2, DSSC/TiO_2-av20, DSSC/TiO_2-av40, DSSC/TiO_2-av60 and DSSC/TiO_2-av100 respectively. On the other hand, the value of charge transfer resistance at the photoanode /electrolyte interface (R_{CT2}) was found to be smaller for the DSSC/TiO_2-av20 (64.70 Ω), then DSSC/TiO_2 (64.70 Ω). The reduced values of R_{CT2} indicate the better electron transport on the surface of photoanodes which resulted in the enhancement of the *J*sc and thus overall conversion efficiency (*η*).

4. Conclusion

The concentration of green extract on TiO_2 NPs plays a crucial role in determining the efficiency of DSSCs, with an optimal concentration range that maximizes light absorption and electron injection while minimizing adverse effects.In summary, spherical TiO_2 NPs were successfully prepared by the reduction of their precursors using different concentration of *Aloe barbadensis miller* leaves extract *by* hydrothermal process for efficient DSSCs. The variation in concentration of *Aloe barbadensis miller* leaves extract massively changes TiO_2 NPs size and thus leads to control the particle size but not changes morphology of TiO_2 NPs. The prepared *Aloe barbadensis miller* leaves extract mediated TiO_2 NPs displays enhanced crystalline nature compared to pure TiO_2 NPs. The as synthesized TiO_2 NPs were applied as photoanodes in the DSSCs after sensitizing with commercial N719 dye. The DSSC (DSSC/TiO_2-av20) based on TiO_2 photoanode prepared with 20 ml concentration of *Aloe barbadensis miller* leaves extract exhibit highest efficiency of 4.3 % and the DSSC (DSSC/TiO_2-av40) based on TiO_2 photoanode prepared with 40 ml concentration of *Aloe barbadensis miller* leaves extract achieved efficiency of 2.6 %, compared to 2.5 % for DSSCs based on the pure TiO_2 photoelectrodes (DSSC/TiO_2). Generally, increasing the concentration of the green extract can enhance the light-harvesting capability of the DSSCs, leading to higher short-circuit current density (Jsc) and overall efficiency. However, there is typically an optimal concentration range beyond which further increases may not necessarily improve the efficiency and could even lead to adverse effects such as aggregation of molecules or increased charge recombination. Thus, finding this optimal concentration often involves experimental optimization and may vary depending on the specific green extract and TiO_2 NPs characteristics.

CRediT authorship contribution statement

Anamika Chaudhari: Visualization, Validation, Methodology, Investigation, Formal analysis, Conceptualization. **Aman Kumar:** Methodology, Investigation, Conceptualization. **Sudhanshu Kumar:** Visualization, Investigation, Formal analysis, Data curation. **Suman Kushwaha:** Writing – review & editing, Writing – original draft, Methodology, Investigation, Funding acquisition, Conceptualization.

Declaration of competing interest

The authors declare the following financial interests/personal relationships which may be considered as potential competing interests: Dr.Suman Kushwaha reports financial support was provided by Banaras Hindu University. If there are other authors, they declare that they have no known competing financial interests or personal relationships that could have appeared to influence the work reported in this paper.

Data availability

Data will be made available on request.

Acknowledgment

The author Suman Kushwaha acknowledge the financial support (seed grant) from Institute of Eminence (IoE) B.H.U., Varanasi. Authors are thankful to Sophisticated Analytical and Technical Help Institute (SATHI) at Banaras Hindu University (BHU) for providing photo electrochemical facilities.

References

[1] A. Yildiz, et al., Efficient iron phosphide catalyst as a counter electrode in dye-sensitized solar cells, ACS Appl. Energy Mater. 4 (10) (2021) 10618–10626.
[2] A. Atilgan, A. Yildiz, Ni-doped TiO_2/TiO_2 homojunction photoanodes for efficient dye-sensitized solar cells, Int. J. Energy Res. 46 (10) (2022) 14558–14569.
[3] A. Atli, A. Yildiz, Opaque Pt counter electrodes for dye-sensitized solar cells, Int. J. Energy Res. 46 (5) (2022) 6543–6552.
[4] K. Salimi, et al., Plasmonic mesoporous core-shell Ag-Au@ TiO_2 photoanodes for efficient light harvesting in dye sensitized solar cells, Sol Energy 193 (2019) 820–827.
[5] C. Altinkaya, et al., Facile fabrication of low-cost low-temperature carbon-based counter electrode with an outstanding fill factor of 73% for dye-sensitized solar cells, Int. J. Energy Res. 44 (4) (2020) 3160–3170.
[6] Y. Kocak, et al., Extraction method dependent performance of bio-based dye-sensitized solar cells (DSSCs), Mater. Res. Express 6 (9) (2019) 095512.
[7] G. Gerischer, H.M.E. Michel-Beyerle, F. Rebentrost, H. Tributsch, Sensitization of charge injection into semiconductors with large band gap, Electrochim. Acta 13 (6) (1968) 1509–1515.
[8] S. Namba, Y. Hishiki, Color sensitization of zinc oxide with cyanine dyes, J. Phys. Chem. 69 (3) (1965) 774–779.
[9] MT. Spitler, M. Calvin, Electron transfer at sensitized TiO_2 electrodes, J. Chem. Phys. 66 (10) (1977) 4294–4305.
[10] B. O'Regan, M. Gratzel, Light induced charge separation in nanocrystalline films, Nature 353 (1991) 737–740.
[11] N.G. Park, J. Van de Lagemaat, A.A. Frank, Comparison of dye-sensitized rutile-and anatase-based TiO_2 solar cells, J. Phys. Chem. B 104 (38) (2000) 8989–8994.
[12] A.J. Frank, N. Kopidakis, J. Van De Lagemaat, Electrons in nanostructured TiO_2 solar cells: transport, recombination and photovoltaic properties, Coord. Chem. Rev. 248 (13–14) (2004) 1165–1179.
[13] O. Carp, C.L. Huisman, A. Reller, Photoinduced reactivity of titanium dioxide, Prog. Solid State Chem 32 (1–2) (2004) 33–177.
[14] M.A Mahshid, M. Sasani Ghamsari, N. Afshar, S. Lahuti, Mixed-phase TiO_2 nanoparticles preparation using sol–gel method, J. Alloys Compd. (2009) 478.

[15] K. Santhi, M. Navaneethan, S. Harish, S. Ponnusamy, C. Muthamizhchelvan, Synthesis and characterization of TiO_2 nanorods by hydrothermal method with different pH conditions and their photocatalytic activity, Appl. Surf. Sci. 500 (2020) 144058.
[16] M.R. Venkatraman, N. Muthukumarasamy, S. Agilan, V. Asokan, D. Velauthapillai, Size controlled synthesis of TiO_2 nanoparticles by modified solvothermal method towards effective photo catalytic and pholtovoltaic applications, Mater. Res. Bull. 97 (2018) 351–360.
[17] N.K. Memon, D.H. Anjum, S.H. Chung, Multiple-diffusion flame synthesis of pure anatase and carbon-coated titanium dioxide nanoparticles, Combust Flame 160 (2013) 1848.
[18] J. MacMullen, Z. Zhang, J. Radulovic, C. Herodotou, M. Totomis, H.N. Dhakal, N. Bennett, Titanium dioxide and zinc oxide nano-particulate enhanced oil-in-water (O/W) facade emulsions for improved masonry thermal insulation and protection, Energy Build 52 (2012) 86.
[19] G. Rajakumar, A.A. Rahuman, S.M. Roopan, V. Khanna, G. Elango, C. Kamaraj, A. A. Zahir, K. Velayutham, Fungus-mediated biosynthesis and characterization of TiO_2 nanoparticles and their activity against pathogenic bacteria, Spectrochim. Acta A 91 (2012) 23.
[20] M. Hudlikar, S. Joglekar, M. Dhaygude, K. Kodam, Green synthesis of TiO2 nanoparticles by using aqueous extract of Jatropha curcas L. latex, Mater. Lett. 75 (2012) 196.
[21] S.M. Roopan, A. Bharathi, A. Prabhakarn, A.A. Rahuman, K. Velayutham, G. Rajakumar, R.D. Padmaja, M. Lekshmi, G. Madhumitha, Efficient phyto-synthesis and structural characterization of rutile TiO_2 nanoparticles using Annona squamosa peel extract, Spectrochim. Acta A 98 (2012) 86.
[22] T. Santhoshkumar, A.A. Rahuman, C. Jayaseelan, G. Rajakumar, S. Marimuthu, A. V. Kirthi, K. Velayutham, J. Thomas, J. Venkatesan, S.K. Kim, A. Pac, Green synthesis of titanium dioxide nanoparticles using Psidium guajava extract and its antibacterial and antioxidant properties, J. Trop. Med. 7 (2014) 968.
[23] K.S. Jamuna, S. Banu, P. Brindha, G.A. Kurian, Nano-scale preparation of titanium dioxide by Desmodium gangeticum root aqueous extract, Ceram. Int. 40 (2014) 11933.
[24] G. Rajakumar, A.A. Rahuman, C. Jayaseelan, T. Santhoshkumar, S. Marimuthu, C. Kamaraj, A. Bagavan, A.A. Zahir, A.V. Kirthi, G. Elango, P. Arora, R. Karthikeyan, S. Manikandan, S. Jose, Solanum trilobatum extract-mediated synthesis of titanium dioxide nanoparticles to control Pediculus humanus capitis, Hyalomma anatolicum anatolicum and Anopheles subpictus, Parasitol. Res. 113 (2014) 469.
[25] G. Rajakumar, A.A. Rahuman, S.M. Roopan, I.M. Chung, K. Anbarasan, V. Karthikeyan, Efficacy of larvicidal activity of green synthesized titanium dioxide nanoparticles using Mangifera indica extract against blood-feeding parasites, Parasitol. Res. 114 (2015) 571.
[26] T. Santhoshkumar, A.A. Rahuman, C. Jayaseelan, A. Pac, Green synthesis of titanium dioxide nanoparticles using Psidium guajava extract and its antibacterial and antioxidant properties, J. Trop. Med. 7 (12) (2014) 968–976.
[27] H. Kaur, S. Kaur, J. Singh, M. Rawat, S. Kumar, Expanding horizon: green synthesis of TiO_2 nanoparticles using Carica papaya leaves for photocatalysis application, Mater. Res. Express 6 (2019) 095034.
[28] S.P. Goutam, G. Saxena, V. Singh, A.K. Yadav, R.N. Bharagava, K.B. Thapa, Green synthesis of TiO_2 nanoparticles using leaf extract of Jatropha curcas L. for photocatalytic degradation of tannery wastewater, Chem. Eng. J. 336 (2018) 386–396.
[29] G. Rajakumar, A.A. Rahuman, B. Priyamvada, V.G. Khanna, D.K. Kumar, P.J. Sujin, Eclipta prostrata leaf aqueous extract mediated synthesis of titanium dioxide nanoparticles, Mater. Lett. 68 (2012) 115–117.
[30] A. Kumar, et al., Biosynthesis of TiO_2 nanostructures using Camellia sinensis extract (polyphenols) and investigation of their execution as photoanodes in photovoltaic device, Surf. Interfaces 47 (2024) 104154.
[31] K. Eshun, Q. He, Aloe vera: a valuable ingredient for the food, pharmaceutical and cosmetic industries—a review, Crit. Rev. Food Sci. Nutr. 44 (2004) 91.
[32] M.D. Boudreau, F.A. Beland, An evaluation of the biological and toxicological properties of Aloe barbadensis (miller), Aloe vera, J. Environ. Sci. Health C 24 (2006) 103.
[33] J.H. Hamman, Composition and applications of Aloe vera leaf gel, Molecules 13 (2008) 1599.
[34] K.S. Venkatesh, S.R. Krishnamoorthi, N.S. Palani, V. Thirumal, S.P. Jose, F. Wang, R. Ilangovan, Facile one step synthesis of novel TiO_2 nanocoral by sol–gel method using Aloe vera plant extract, Indian J. Phys. 89 (2015) 445–452.
[35] K.G Rao, C.H. Ashok, K. Venkateswara Rao, C.S. Chakra, P. Tambur, Green synthesis of TiO_2 nanoparticles using Aloe vera extract, Int. J. Adv. Res. Phys. Sci. 2 (1A) (2015) 28–34.
[36] S. Gowri, R. Rajiv Gandhi, S. Senthil, J. Suresh, M. Sundrarajan, Enhancing antimicrobial activity of biotemplated TiO_2 nanoparticles using aloe vera plant extract, J. Bionanosci. 10 (3) (2016) 181–190.
[37] J. Rajkumari, C.M Magdalane, B. Siddhardha, J. Madhavan, G. Ramalingam, N. Abdullah Al-Dhabi, M. Valan Arasu, A.K.M. Ghilan, V. Duraipandiayan, K. Kaviyarasu, Synthesis of titanium oxide nanoparticles using Aloe barbadensis mill and evaluation of its antibiofilm potential against Pseudomonas aeruginosa PAO1, J. Photochem. Photobiol. B Biol. 201 (2019) 111667.
[38] N.K. Ahmed, A. Abbady, Y.A. Elhassan, A.H. Said, Green synthesized titanium dioxide nanoparticle from aloe vera extract as a promising candidate for radiosensitization applications, Bionanoscience 13 (2) (2023) 730–743.
[39] A. Doaa, et al., Novel greenly synthesized titanium dioxide nanoparticles compared to liposomes in drug delivery: in vivo investigation on Ehrlich solid tumor model, Heliyon 7 (2021) e07370.
[40] M. Santiago, R. Daniela, T. Agustín, Green Synthesis of Titanium Oxide Nanoparticles Using Natural Extracts, J. Mater. Sci. Chem. Eng. 11 (2023) 29–40.
[41] M.S. Hanafy, D. Abdel Fadeel, M. Elywa, N. Kelany, Green synthesis and characterization of TiO_2 nanoparticles using Aloe vera extract at different pH value.,, Sci. J. King Faisel Univ. 21 (1) (2020) 103–110.
[42] S. Bhullar, N. Goyal, S. Gupta, Rapid green-synthesis of TiO_2 nanoparticles for therapeutic applications, RSC Adv 11 (48) (2021) 30343–30352.
[43] K.G. Rao, C.H. Ashok, K.V. Rao, C.S. Chakra, P. Tambur, Green synthesis of TiO2 nanoparticles using Aloe vera extract.Green synthesis of TiO_2 nanoparticles using Aloe vera extract, Int. J. Adv. Res. Phys. Sci 2 (1A) (2015) 28–34.
[44] K.S. Venkatesh, S.R. Krishnamoorthi, N.S. Palani, V. Thirumal, S.P. Jose, F. M. Wang, R. Ilangovan, Facile one step synthesis of novel TiO_2 nanocoral by sol–gel method using Aloe vera plant extract, Indian J. Phys. 89 (2015) 445–452.
[45] A. Femenia, et al., Compositional features of polysaccharides from Aloe vera (Aloe barbadensis Miller) plant tissues, Carbohydr. Polym. 39 (2) (1999) 109–117.
[46] K. Eshun, Q. He, Aloe vera: a valuable ingredient for the food, pharmaceutical and cosmetic industries—a review, Crit. Rev. Food Sci. Nutr. 44 (2) (2004) 91–96.
[47] S.P. Chandran, M. Chandhary, R. Pasricha, A. Ahmad, M. Sastry, Synthesis of Gold Nanotriangles and Silver Nanoparticles Using *Aloevera* Plant Extract, Biotechnol. Prog. 22 (2006) 577.
[48] A. Yildiz, et al., Effect of grain size and strain on the bandgap of glancing angle deposited AZO nanostructures, J. Mater. Sci. Mater. Electron. 26 (2015) 5952–5957.
[49] T. Serin, et al., Electron transport in Al-Cu co-doped ZnO thin films, J. Appl. Phys. 121 (9) (2017).
[50] M. Hossain, S. Ahmed, Easy and green synthesis of TiO_2 (Anatase and Rutile): Estimation of crystallite size using Scherrer equation, Williamson-Hall plot, Monshi-Scherrer Model, size-strain plot, Halder-Wagner Model, Results Mater 20 (2023) 100492.
[51] Dunlap, R.A., X-ray Difraction Techniques. (2018); 2–16.
[52] F. Li, Y. Gu, Improvement of performance of dye-sensitized solar cells by doping Er_2O_3 into TiO_2 electrodes, Mater. Sci. Semicond. Process. 15 (2012) 11–14.
[53] W.F. Zhang, Y.L. He, M.S. Zhang, Z. Yin, Q. Chen, Raman scattering study on anatase TiO_2 nanocrystals, J. Phys. D Appl. Phys. 33 (8) (2000) 912.
[54] S. Pazokifard, S.M. Mirabedini, M. Esfandeh, M. Mohseni, Z. Ranjbar, Silane grafting of TiO_2 nanoparticles: dispersibility and photoactivity in aqueous solutions, Surf. Interface Anal 44 (2012) 41–47.
[55] J.G. Yu, H.G. Yu, B. Cheng, C. Trapalis, Effects of calcination temperature on the microstructures and photocatalytic activity of titanate nanotubes, J. Mol. Catal. A 249 (1–2) (2006) 135–142.
[56] T. Alammar, H. Noei, Y. Wang, A.V. Mudring, Mild yet phase-selective preparation of TiO_2 nanoparticles from ionic liquids–a critical study, Nanoscale 5 (17) (2013) 8045–8055.
[57] S.A.A. Shah, M.H. Sayyad, N. Nasr, R.A. Toor, S. Sajjad, H. Elbohy, Q. Qiao, Photovoltaic performance and impedance spectroscopy of a purely organic dye and most common metallic dye based dye-sensitized solar cells, J. Mater. Sci. Mater. Electron. 28 (2017) 6552–6559.
[58] Z.Q. Li, Y.P. Que, L.E. Mo, W.C. Chen, Y. Ding, Y.M. Ma, L. Jiang, L.H. Hu, S.Y. Dai, One-Pot Synthesis of Mesoporous TiO_2 Micropheres and Its Application for High-Efficiency Dye-Sensitized Solar Cells, ACS Appl. Mater. Interfaces 7 (20) (2015) 10928–10934.
[59] A. Kumar, A. Chaudhari, S. Kumar, S. Kushwaha, Biosynthesis of TiO_2 nanostructures using Camellia sinensis extract (polyphenols) and investigation of their execution as photoanodes in photovoltaic device, Surf. Interfaces 47 (2024) 104154.
[60] S. Singh, I. Chandra Maurya, A. Tiwari, P. Srivastava, L. Bahadur, Green synthesis of TiO_2 nanoparticles using Citrus limon juice extract as a bio-capping agent for enhanced performance of dye-sensitized solar cells, Surf. Interfaces 28 (2022) 101652.
[61] R. Senthamarai, V. Madurai Ramakrishnan, B. Palanisamy, S. Kulandhaivel, Synthesis of TiO_2 nanostructures by green approach as photoanodes for dye-sensitized solar cells, Int. J. Energy Res. 45 (2) (2021) 3089–3096.
[62] I.C. Maurya, S. Singh, S. Senapati, P. Srivastava, L. Bahadur, Green synthesis of TiO_2 nanoparticles using Bixa orellana seed extract and its application for solar cells, Solar Energy 194 (2019) 952–958.
[63] A.M. Sharif, Md Ashrafuzzaman, A. Kalam, A.G. Al-Sehemi, P. Yadav, B. Tripathi, M. Dubey, G. Du, Green synthesis of pristine and Ag-doped TiO_2 and investigation of their performance as photoanodes in dye-sensitized solar cells, Materials 16 (17) (2023) 5731.
[64] S.U. Ekar, G. Shekhar, Y.B. Khollam, P.N. Wani, S.R. Jadkar, M. Naushad, M. G. Chaskar, et al., Green synthesis and dye-sensitized solar cell application of rutile and anatase TiO_2 nanorods, J. Solid State Electrochem. 21 (2017) 2713–2718.
[65] R.A. Metwally, J. El Nady, S. Ebrahim, A. El Sikaily, N.A. El-Sersy, S.A. Sabry, H. A. Ghozlan, Biosynthesis, characterization and optimization of TiO_2 nanoparticles by novel marine halophilic Halomonas sp. RAM2: application of natural dye-sensitized solar cells, Microb. Cell Fact. 22 (1) (2023) 78.
[66] P. Singh, S. Sharma, P. Srivastava, Natural Saccharum officinarum (sugarcane) juice assisted TiO_2 nanoparticle synthesis for high performance dye-sensitized solar cell.,, Opt Mater 147 (2024) 114685.
[67] A. Kumar, A. Chaudhari, S. Kumar, S. Kushwaha, S. Mandal, Comparative study of natural and synthetic dyes in DSSCs: An experimental and computational approach, Phys. B Condensed Matter (2024) 415978.
[68] D.K. Roh, W.S. Chi, H. Jeon, S.J. Kim, J.H. Kim, High efficiency solid-state dye-sensitized solar cells assembled with hierarchical anatase pine tree-like TiO_2 nanotubes, Adv. Funct. Mater. 24 (2014) 379–386.

[69] J.Y. Zhao, J.X. Yao, Y.Z. Zhang, M. Guli, L. Xiao, Effect of thermal treatment on TiO_2 nanorod electrodes prepared by the solvothermal method for dye-sensitized solar cells: Surface reconfiguration and improved electron transport, J. Power Sources 255 (2014) 16–23.

[70] J. Peng, H.H. Lin, C.T. Lee, C.M. Tseng, V. Suryanarayanan, R. Vittal, K.C. Ho, Hierarchically assembled microspheres consisting of nanosheets of highly exposed (001)-facets TiO_2 for dye-sensitized solar cells,, RSC Adv 6 (17) (2016) 14178–14191.

[71] R.S. Dubey, S.R. Jadkar, A.B. Bhorde, Synthesis and characterization of various doped TiO_2 nanocrystals for dye-sensitized solar cells, ACS Omega 6 (5) (2021) 3470–3482.